Chapter 14

Experimental Investigation of Power Requirements for Wind Turbines Electrothermal Anti-icing Systems

Oloufemi Fakorede, Hussein Ibrahim, Adrian Ilinca and Jean Perron

Additional information is available at the end of the chapter

http://dx.doi.org/10.5772/63449

Abstract

Atmospheric icing effects is a critical issue for wind farms in Nordic regions; it is responsible for production losses, shortens the equipment's lifetime, and increases safety risks. Electrothermal anti-icing is one of the existing techniques of ice mitigation, and its energy consumption for wind turbines has been numerically investigated over the years but never fully validated experimentally in the literature. In this work, we aimed to determine the energy consumption for anti-icing systems based solely on experimental investigations. Our methodology is to quantify the energy required to protect a custom-built NACA 0012 airfoil from ice buildup in a wind tunnel. The results are extrapolated to a full-scale wind turbine.

Keywords: wind turbines, anti-icing, ice mitigation systems, energy consumption, electrothermal anti-icing systems

1. Introduction

To perform anti-icing, knowing the energy required to prevent ice buildup on the wind turbine's blade is the most important parameter for a wind farm operator. It can be used to select the most suitable ice protection system for a given site and to decide whether or not to operate wind turbines during icing events. There are a few softwares, primarily designed for aeronautics, such as LEWICE, TURBICE, and FENSAP-ICE based on computational fluid dynamics (CFD) methods that can be used for modeling anti-icing for wind turbine blades. They require a certain level of expertise to be used. However, more importantly, there are very

few research results in the literature for anti-icing experiments on full-scale wind turbines. These results are essential for validation and improvement of existing numerical models.

Our approach is to experimentally investigate the power requirement for anti-icing on a NACA 0012 airfoil partially equipped with resistive heaters and instrumented with fluxmeters and thermocouples. Based on wind tunnel measurements, correlations are developed between the anti-icing energy flux and the airflow wind speed for a given temperature and liquid water content. Finally, under some assumptions, we use these correlations to evaluate the anti-icing power requirements for a full-scale wind turbine. Our experiments have been conducted in the icing wind tunnel of the Anti-icing Materials International Laboratory at the University of Québec at Chicoutimi.

2. Wind turbine Icing

Ice accretion on wind turbine blades can affect both the energy production and the lifetime of the wind turbine. Ice accumulation on blades reduces wind turbine power due to airfoil shape alteration and increased surface roughness [1]. This disrupts the airflow, increases drag, and reduces lift [2, 3, 4]. In severe meteorological conditions, ice accretion on the blades can cause downtime for days or weeks at a time [5]. An imbalanced ice load on the blades can increase their vibrations and reduce the wind turbine's lifetime [6, 7]. Also, ice blocks fall represent a risk for both staff and facilities in the vicinity. In certain cases, the ice on the blade can delay the stall causing a power surge that can damage components and cause fires [8]. In areas subjected to frequent icing events, an ice mitigation strategy is mandatory in order to reduce production losses [9, 10].

To overcome the effects of icing, wind farm operators have generally two solutions. The first is to stop the wind turbine during icing events. With this strategy, the turbines must remain stopped until there is no more ice on the blades; this can have a strong impact on the profitability of a wind plant if icing events are frequent because the recovery time is often very long. The second alternative is to install an ice protection device. Several more or less complex approaches and technologies have been implemented over the years in wind farms. Currently, wind turbines designed to be much better adapted to cold climate regions and equipped with ice protection systems are available in the market.

Ice protection systems can be regrouped in two categories: anti-icing and de-icing. Anti-icing systems prevent ice buildup at the surface of the blade while de-icing systems remove accumulated ice from the surface of the blade [11].

There are several types of ice protection systems using various technologies for mitigating ice accretion on wind-turbine blades. These technologies can be passive (ice-phobic/hydrophobic coatings, thermal coatings such as black paint, etc.) or active (antifreeze coolants, pneumatic and expulsive techniques, hot air injection, resistive heaters, microwaves or infrared heating, etc.) [12, 13]. Heating the wind turbine's blade is currently the most efficient protection technique against ice accretion. It can be achieved by driving hot air inside the blade or by

http://dx.doi.org/10.5772/63449

installing resistive heaters on or in the blade. Driving hot air along a high diameter rotor results in important energy loss. Besides, retrofit is not possible with the hot air system. Therefore, resistive heaters installed on the outer surface of the blade seems to be the most suitable technique for most applications.

3. Methodology

There are two anti-icing systems using resistive coatings. The first one consists in heating the surface enough to evaporate the impinging droplets; it is the evaporative anti-icing. This technique requires a lot of energy, and the effects of the heat on the blade lifetime are unknown at this time. The second approach consists in heating the droplets enough to avoid accretion both on impact and during runback; it is the wet running anti-icing. This approach requires transferring an additional energy to the droplet in order to prevent the freezing when it streams along the blade. Our experimentation is based on the second approach.

For the experimental work, we use a rectangular NACA 0012 airfoil blade with a constant section of 0.254 m and length of 0.381 m. The airfoil is covered with resistive heaters and instrumented with fluxmeters and thermocouples. For various airflow wind speeds, temperatures, and liquid water contents, we measure the heating energy required to maintain the airfoil surface temperature at 5°C determined as a threshold for keeping the runback water in liquid form. The data are processed to find correlations that will help to extrapolate the anti-icing energy consumption of an operating full-scale wind turbine blade.

4. Fundamentals of power requirements

4.1. Sensible heating

The sensible heating is the energy required to heat up the impinging droplets in order to keep them in a liquid state. Part of this energy serves to heat up the runback water and avoid secondary icing. If we assume that the droplets are heated from their initial temperature to the surface temperature, the sensible heating can be expressed by

$$\dot{q}_{\text{sens}} = \dot{q}_{\text{imp}} = \dot{m}_{\text{imp}} \cdot C_{p,w}\left(T_{\text{s}} - T_{\infty}\right) \tag{1}$$

The impinging mass flow of droplets is the amount of water per unit of time and surface that can be caught by the airfoil. It is also known as the intensity of ice accretion and identified according to the formula [14]:

$$\dot{m}_{imp} = V \cdot LWC \cdot E \tag{2}$$

The collection efficiency E can be taken as the average of local collection efficiencies around the airfoil.

4.2. Kinetic heating

Kinetic heating is the gain of energy due to the velocity of the droplets and is given by [15]

$$\dot{q}_{kin} = \dot{m}_{imp} \frac{V_\infty^{\ 2}}{2} \tag{3}$$

4.3. Convective energy loss

The convective heat loss is given by [15]

$$\dot{q}_{conv} = h\left(T_s - T_\infty\right) \tag{4}$$

The convective heat transfer coefficient h is an averaged value. It is usually computed at the tip of the blade section (highest distance from the nacelle).

4.4. Evaporative energy loss

Even if the anti-icing strategy does not consist in the evaporation of the impinging droplets, the heat at the airfoil surface is high enough to evaporate a fraction of the impinging water. The evaporated heat loss can be estimated with [15]

$$\dot{q}_{evap} = \frac{0.622 \cdot h \cdot 2.5 \cdot 10^6}{C_{p,a} \cdot L_{evap}^{\ 2/3} \cdot p_\infty^0} 27.03 \cdot \left(T_s - T_\infty\right) \tag{5}$$

4.5. Aerodynamic heating

Aerodynamic heating is due to the friction between the droplet and the air [16]:

$$\dot{q}_{aero} = h \frac{r_c V_\infty^{\ 2}}{2C_{p,a}} \tag{6}$$

with

http://dx.doi.org/10.5772/63449

$$r_c = \begin{cases} \left(\frac{C_{p,a}\mu}{k_a}\right)^{\frac{1}{2}} = Pr^{1/2} & \left(laminar\,boundary\right) \\ \left(\frac{C_{p,a}\mu}{k_a}\right)^{\frac{1}{3}} = Pr^{1/3} & \left(turbulent\,boundary\right) \end{cases} \tag{7}$$

4.6. Energy balance

The energy balance equation is given by

$$\left|\dot{q}_{anti}\right| + \left|\dot{q}_{aero}\right| + \left|\dot{q}_{kin}\right| = \left|\dot{q}_{conv}\right| + \left|\dot{q}_{sens}\right| + \left|\dot{q}_{evap}\right| \tag{8}$$

5. Experimental investigations

5.1. Icing wind tunnel

AMIL's icing wind tunnel is a closed-loop, low-speed, refrigerated wind tunnel which is able to operate at negative temperatures. The refrigeration system is capable of varying the air temperature between −20 and 20°C by passing it through a 1.6 m × 1.6 m heat exchanger powered by a compressor and a glycol pump. A fan connected to a motor allows for an empty section to reach flow rates up to 31 kg/s at an air temperature of 22°C.

The icing wind tunnel has two test sections. The smaller one measure 0.5 m wide by 0.6 m high and can be used to perform experiments at wind speeds up to 37 m/s at ambient temperature. The second test section is 0.91 m wide by 0.76 m high and can reach wind speeds up to 86 m/

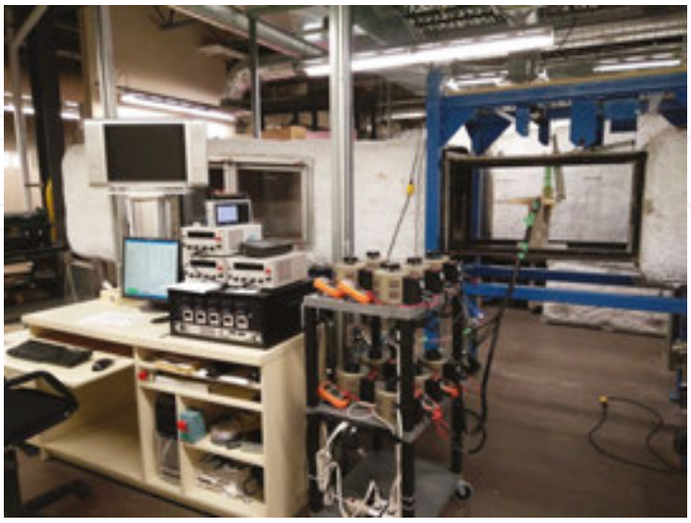

Figure 1. Experimental setup in the small section of the icing wind tunnel.

s at ambient temperature. Experiments in this study have been done using the small section (**Figure 1**).

5.2. Experimental setup

The airfoil has been made of 2.54-mm-thick fiberglass resin. It is equipped with 10 resistive heaters pasted on the external surface of the upper surface (**Figure 2**).

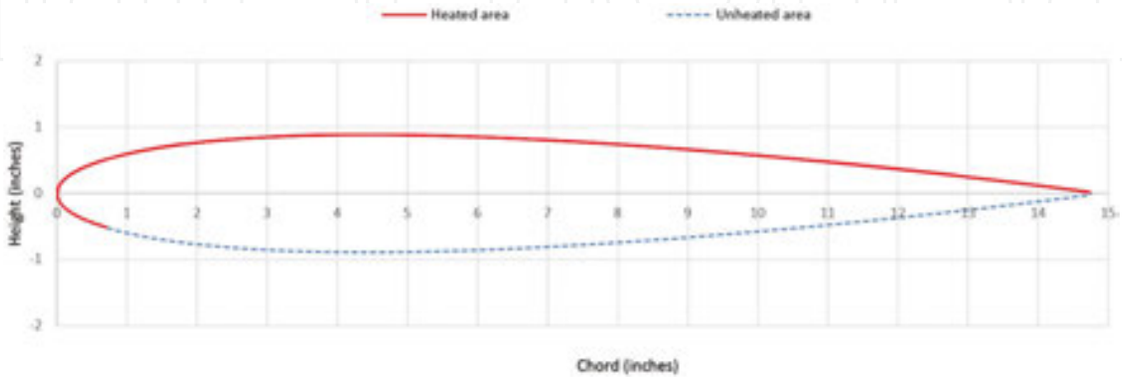

Figure 2. Resistive heater distribution along the experimental airfoil.

A thermocouple is placed between the surface of the airfoil and each resistive heater. Another thermocouple is placed inside the airfoil right under the external thermocouple. In addition, a fluxmeter is pasted above each resistive heater; these fluxmeters give the outgoing energy flux and an additional indication of the surface temperature. Each heater is powered individually by an independent power source. The setup has a total of 20 thermocouples, 10 fluxmeters, 10 resistive heaters, and 10 power sources (**Figure 3**).

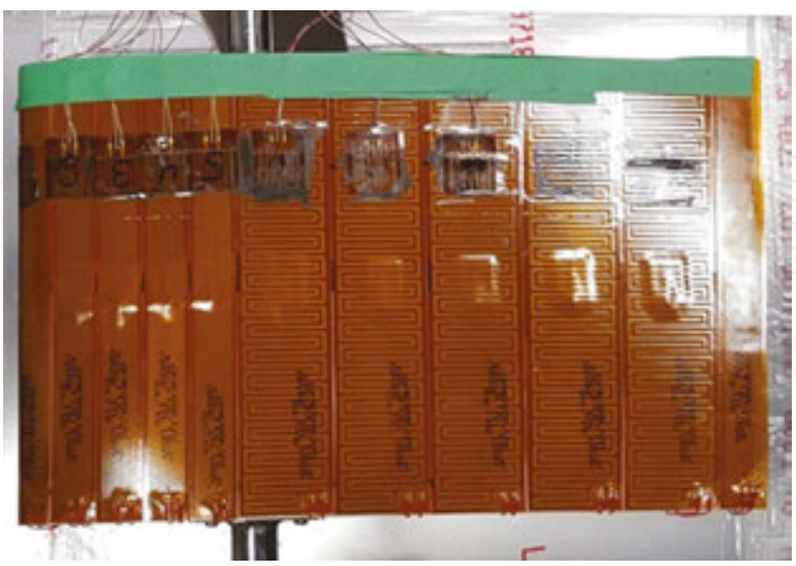

Figure 3. Upper view of the NACA0012 airfoil.

http://dx.doi.org/10.5772/63449

5.3. Energy consumption

We have conducted 30 experiments at five different wind speeds (10, 15, 20, 25, and 30 m/s), two different temperatures (−10 and −15°C), and three different values of liquid water content. The surface temperature in each experiment has been fixed to 5°C and the angle of attack is 0°.

For the first set of experiments, there was no precipitation (dry air):

$$\dot{q}_{anti\_exp} = \dot{q}_{dry} \tag{9}$$

These experiments quantified the convective effects. **Figure 4** shows the variation of $\dot{q}_{\mathrm{dry}}$ with the airflow wind speed.

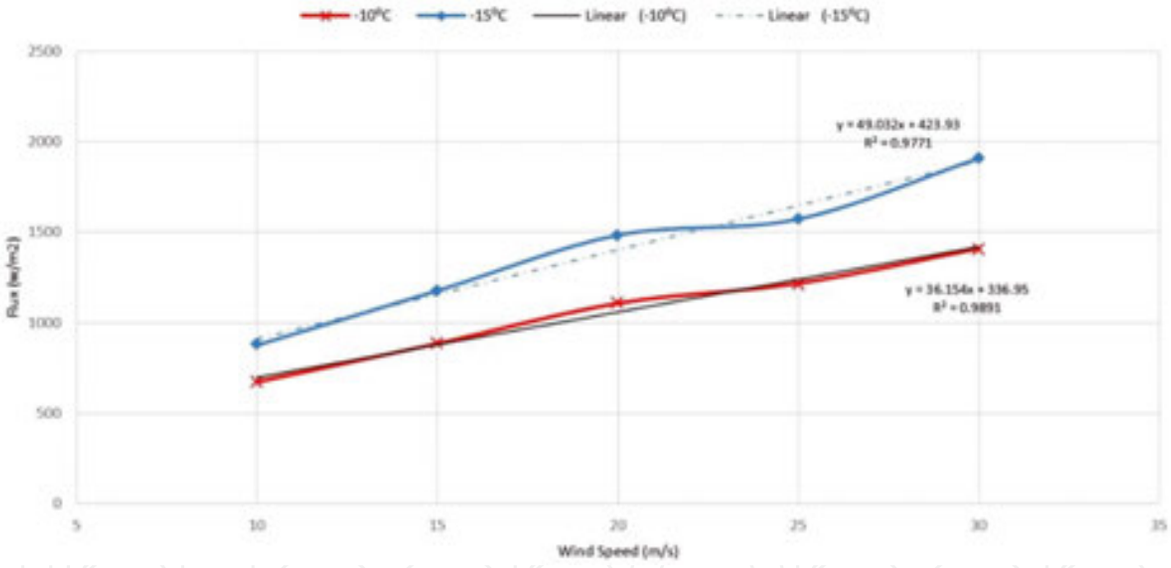

Figure 4. $\dot{q}_{\mathrm{dry}}$variation with the wind speed (LWC = 0 g/m^3).

In the second set of experiments, we fixed the airflow temperature to −10°C and added water droplets to the airflow (wet air):

$$\dot{q}_{\mathrm{anti\_exp}} = \dot{q}_{\mathrm{dry}} + \dot{q}_{\mathrm{wet}} \tag{10}$$

The different values of liquid water contents experimented are 0.3 and 0.9 g/m^3. **Figure 5** shows the variation of $\dot{q}_{\mathrm{wet}}$ with the airflow wind speed.

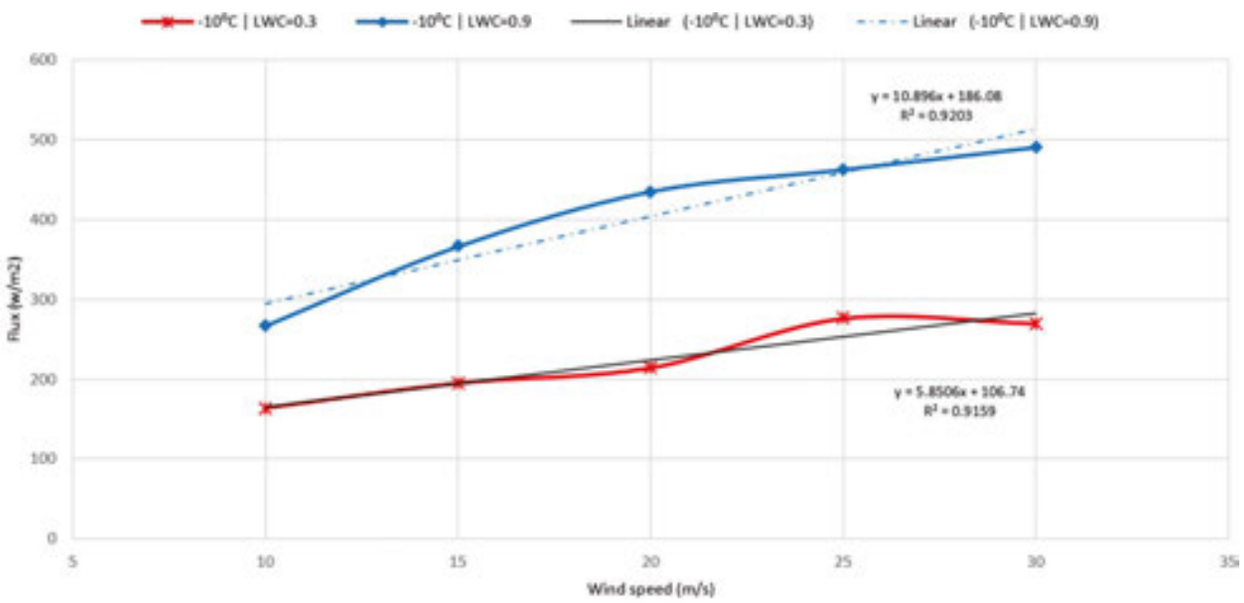

Figure 5. $\dot{q}_{\text{wet}}$variation with the wind speed (LWC = 0.3 g/m^3 and LWC = 0.9 g/m^3) at temperature −10°C.

Finally, we repeat the wet experiments for an airflow temperature of −15°C. **Figure 6** shows the variation of $\dot{q}_{\text{wet}}$ with the airflow wind speed.

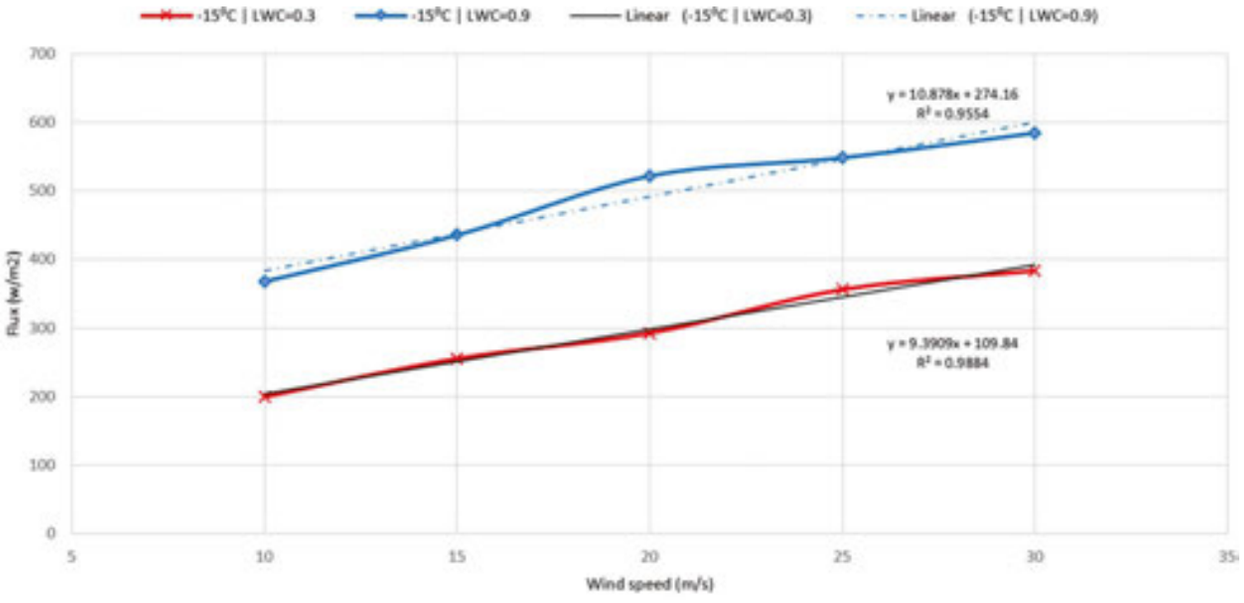

Figure 6. $\dot{q}_{\text{wet}}$ variation with the wind speed (LWC=0.3 g/m^3 and LWC=0.9 g/m^3) at temperature −15°C.

The graphs of $\dot{q}_{\text{wet}}$ and $\dot{q}_{\text{dry}}$, between the ranges of 10 and 30 m/s, can be approximated by linear functions with a very good precision. Thus, under those conditions, we can deduce the following correlations for required anti-icing energy flux.

http://dx.doi.org/10.5772/63449

	LWC = 0 g/m³	**LWC = 0.3 g/m³**	**LWC = 0.9 g/m³**
$T = -10°C$	$\dot{q}_{anti} = 36.154 \cdot V + 336.95$	$\dot{q}_{anti} = (36.154 \cdot V + 336.95) + (5.8506 \cdot V + 106.74)$	$\dot{q}_{anti} = (36.154 \cdot V + 336.95) + (10.896 \cdot V + 186.08)$
$T = -15°C$	$\dot{q}_{anti} = 49.032 \cdot V + 336.95$	$\dot{q}_{anti} = (49.032 \cdot V + 336.95) + (9.3909x + 109.84)$	$\dot{q}_{anti} = (49.032 \cdot V + 336.95) + (10.878 \cdot V + 274.16)$

Table 1. Experimental anti-icing flux correlations.

6. Extrapolation to a full-scale wind turbines

To extrapolate the results presented in the previous section to a full-scale wind turbine, we do the following assumptions:

- Linear approximations of $\dot{q}_{wet} = f(V)$ and $\dot{q}_{dry} = f(V)$ are good for wind speeds between 30 and 80 m/s.
- The turbulence effects around the experimental setup and the wind turbine on site are similar.
- The wind turbine is composed of NACA 0012 blades (3) at an angle of attack of 0°.
- The efficiency of the experimental setup is the same as the efficiency of the anti-icing device installed on the wind turbine.

6.1. Chord distribution

The chord distribution is based on the NREL 5MW reference wind turbine for offshore development [17]. We defined the chord distribution used in our study as follows:

	r*/*R	**Chord/*R***
-	0.00	0.02
Zone 1 (hub)	0.02	0.02
Zone 2	0.05	0.06
Zone 3	0.19	0.07
Zone 4	0.26	0.08
Zone 5	0.96	0.03
Zone 6	1.00	0.02

Table 2. Blade discretization.

The graphical normalized chord distribution is shown in **Figure 7**.

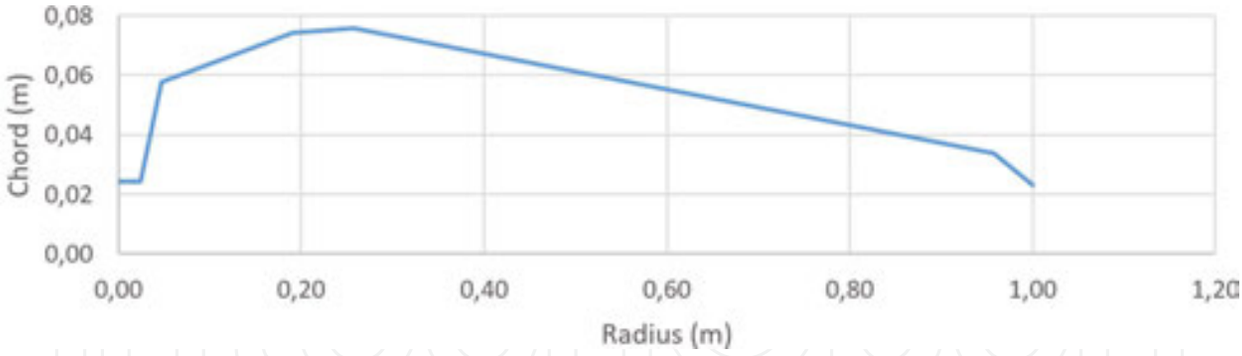

Figure 7. Chord distribution for a 1-m-long blade.

6.2. Wind speed distribution

The relative airflow wind speed V along the blade is given by

$$V(r) = \sqrt{V_\infty{}^2 + (r\omega)^2} \tag{11}$$

with

$$\omega = \frac{V_\infty \cdot \lambda}{R} \tag{12}$$

				Tair = −10°C		
				LWC 0 g/m³	**LWC 0.3 g/m³**	**LWC 0.9 g/m³**
	Radius (m)	Tip speed ratio	Output (KW)	Anti-icing power (KW)		
ENERCON E40	20	5.8	600	130	466	529
Vestas V47	23.5	4.3	660	149	538	612
Vestas V66	33	4.6	1650	300	1100	1250
Vestas V80	40	4.66	2000	450	1630	1850
Vestas V90	45	5.05	3000	600	2160	2460
Vestas V100	50	4.68	2750	710	2550	2910
Vestas V120	60	6.5	4500	1260	4250	5120

Table 3. Extrapolated anti-icing power requirements at −10°C.

http://dx.doi.org/10.5772/63449

6.3. Results

For each zone of the blade determined in Section 6.1, we compute the average value of $\dot{q}_{anti}$ by integrating its expression (**Table 1**) with respect to the radius r. The anti-icing power requirement for each zone is found by multiplying the average $\dot{q}_{anti}$ by the zone's surface (for both intrados and extrados). The total power anti-icing for the wind turbine is summation of the anti-icing power for each zone multiplied by the number of blades. The extrapolation results for seven wind turbines [18–22] are presented in **Tables 3** and **4**.

				Tair = −15°C		
				LWC 0 g/m³	**LWC 0.3 g/m³**	**LWC 0.9 g/m³**
	Radius (m)	Tip speed ratio	Output (KW)	Anti-icing power (KW)		
ENERCON E40	20	5.8	600	173	625	682
Vestas V47	23.5	4.3	660	198	718	792
Vestas V66	33	4.6	1650	400	1470	1620
Vestas V80	40	4.66	2000	600	2180	2400
Vestas V90	45	5.05	3000	800	2900	3170
Vestas V100	50	4.68	2750	940	3410	3750
Vestas V120	60	6.5	4500	1680	6080	6600

Table 4. Extrapolated anti-icing power requirements at −15°C.

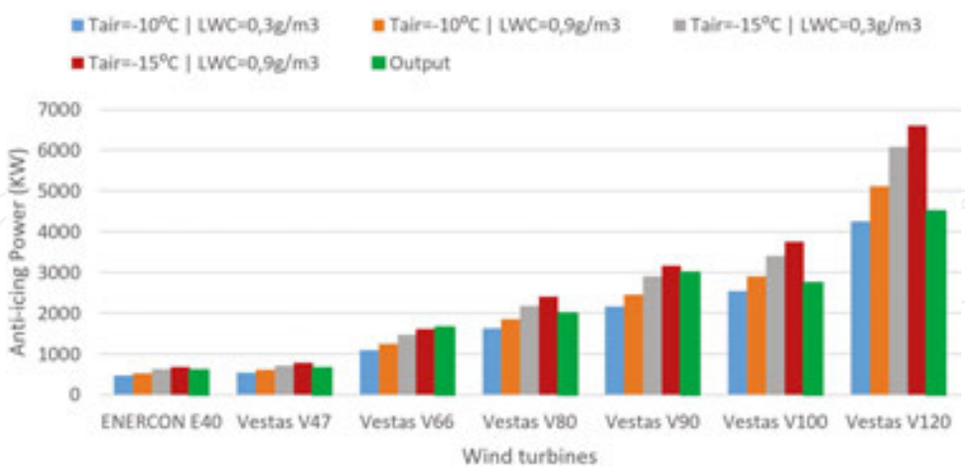

Figure 8. Histogram of the extrapolated anti-icing power requirements.

At first glance, we note that the anti-icing power consumption is sometimes higher than the nominal output power of the wind turbine (**Figure 8**). In such conditions, stopping the wind turbines is a better alternative. Plotting the anti-icing energy in terms of the percentage of the

nominal output power (**Figure 9**) showed that the anti-icing operation consumes more than 50% of the nominal output power.

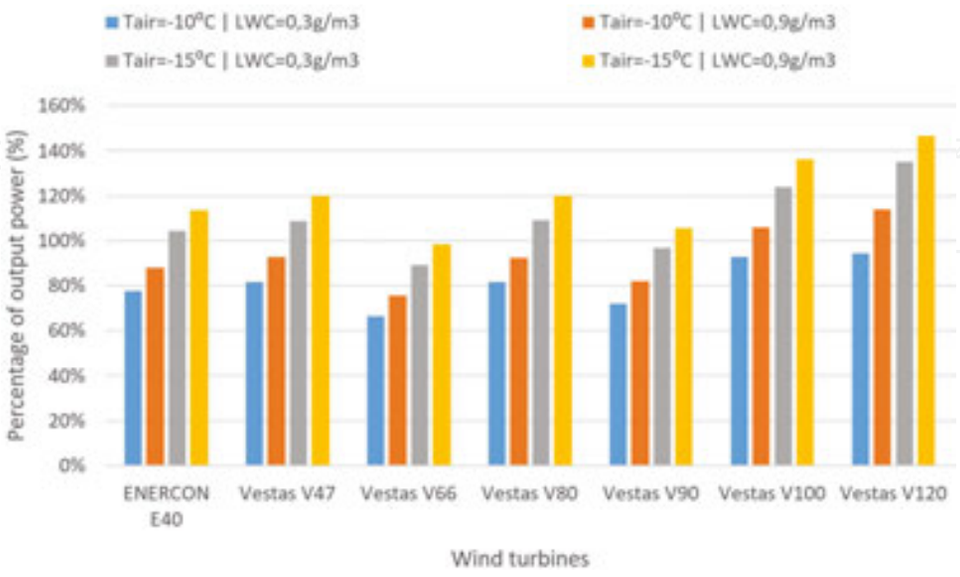

Figure 9. Power requirements in percentage of the nominal output power.

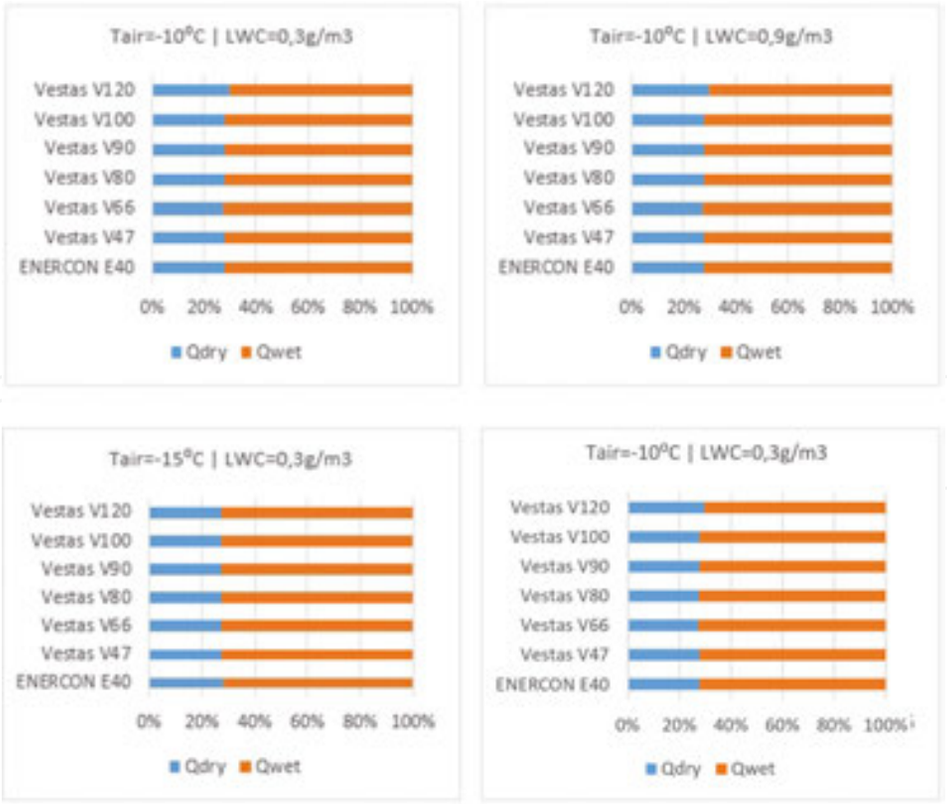

Figure 10. Fraction of Q_{dry} and Q_{wet} in the anti-icing power consumption.

http://dx.doi.org/10.5772/63449

Figure 10 displays the fraction of Q_{dry} and Q_{wet} in the anti-icing energy. It shows that Q_{dry} is at most 30% of the total anti-icing energy. It also means that the convective effects are approximately 30%, and the rest of the energy is lost to the water droplets.

7. Conclusion

In this chapter, we have introduced the effects of the icing on wind turbines and investigated the anti-icing power requirements of a full-scale wind turbine. Our methodology was to build a section of NACA 0012 airfoil covered externally by resistive heaters and instrumented with thermocouples and fluxmeters. We assembled the airfoil and conducted anti-icing tests in the Anti-icing Materials International Laboratory wind tunnel. The measured data have been used to establish correlations between the anti-icing energy and the airflow wind speed around the airfoil. Under some reasonable assumptions, we used these correlations to estimate the anti-icing power consumption for full-scale wind turbines.

The extrapolated power consumption showed that the anti-icing consumed a considerable amount of energy that can exceed the nominal output of the wind turbine itself. In reality, the anti-icing power consumption should be higher than the values that we extrapolated because

- The NACA 0012 is slimmer than the wind turbines airfoil.
- The wind turbine angle of attack is above 0°.

Thus, the blades collect more water droplets and consume more energy. Nevertheless, the work presented in this chapter proves that anti-icing for wind turbines is not a viable solution to mitigate icing effects. The correlation presented in this chapter can also be used for anti-icing on heated flat surfaces.

Given that wind turbines are designed to be more robust and to be able to withstand significant ice loads, then the de-icing seems to be a more promising strategy. This work is the first part of a project on the estimation and control of mass and heat transfers during the anti-icing and de-icing of wind turbines. The project, motivated by the need of the wind industry, answers some issues related to anti-icing strategy and its feasibility. The results are useful for the choice, design, and control of de-icing/anti-icing systems.

8. Abbreviations and acronyms

AMIL: Anti-Icing Materials International Laboratory

CFD: computational fluid dynamics

$\dot{m}_{imp}$: impingement water, kg

E: collection efficiency

C_p: heat capacity, J/(kg K)

NACA: National Advisory Committee for Aeronautics

Q: heating power, W

$\dot{q}$: heating flux, W/m^2

$\dot{q}_{anti}$: anti-icing energy, W/m^2

T_s: surface temperature, K

T_∞: free stream temperature, K

V_∞: free stream velocity, m/s

V: relative stream velocity, m/s

LWC: liquid water content, kg/m^3

h: thermal convection coefficient, W/(m K)

r_c: recovery factor

L_{evap}: latent heat of evaporation, J/kg

$\dot{q}_{dry}$: experimental convective heating, W/m^2

$\dot{q}_{wet}$: experimental water heating, W/m^2

$\dot{q}_{anti\_exp}$: experimental anti-icing energy, W/m^2

$\dot{q}_{sens}$: sensible heating, W/m^2

$\dot{q}_{imp}$: impinging droplet heating, W/m^2

$\dot{q}_{kin}$: kinetic heating, W/m^2

$\dot{q}_{conv}$: convective energy, W/m^2

$\dot{q}_{evap}$: evaporative energy, W/m^2

$\dot{q}_{aero}$: aerodynamic heating, W/m^2

p_∞^0: atmospheric pressure, Pa

k_a: thermal conductivity of air, W/(m K)

μ: dynamic viscosity, kg/(m s)

Pr: Prandtl number

R: blade radius, m

λ: tip speed ratio

ω: rotor velocity, rpm

$\dot{q}_{anti}$: anti-icing energy (W/m^2)

NREL: National Renewable Energy Laboratory

Author details

Oloufemi Fakorede[1], Hussein Ibrahim[2], Adrian Ilinca[3*] and Jean Perron[1]

*Address all correspondence to: Adrian_Ilinca@uqar.ca

1 University of Quebec at Chicoutimi, 555 boulevard de l'Université, QC, Canada

2 TechnoCentre éolien, 70 rue Bolduc, Gaspé, QC, Canada

3 University of Quebec at Rimouski, 300 allée des ursulines, Rimouski, QC, Canada

References

[1] E. Sagol, M. Reggio and A. Ilinca, Issues concerning roughness on wind turbine blades, vol. 23, Renewable and Sustainable Energy Reviews, 2013, pp. 514–525.

[2] W. J. Jasinski, S. C. Noe, M. S. Selig and M. B. Bragg, Wind turbine performance under icing conditions, Journal of Solar Energy Engineering, 1998, vol. 120, no 1, pp. 60–65.

[3] O. Fakorede, J. Perron, A. Ilinca and H. Ibrahim, Modelling ice accretion and its effects on wind turbine blades, Wind turbines: types, design and efficiency, ISBN: 978-162-808-891-5, NY: Nova Science Publishers, Inc., 2013.

[4] P. Suke, Analysis of heating systems to mitigate ice accretion on wind-turbine blades (Master's thesis of Applied Science in Engineering). Hamilton, Ontario: McMaster University; January 2014.

[5] M. Homola, Impacts and causes of icing on wind turbines, Navrik University College Report, 2005.

[6] P. Frohboese and A. Anders, Effects of icing on wind turbine fatigue loads, vol. 75, I. Publishing, Ed., Journal of Physics: Conference Series (Vol. No. 1, p. 012061), 2007.

[7] N. Dalili, A. Edrisy and R. Carriveau, A review of surface engineering issues critical to wind turbine performance, vol. 13(2), Renewable and Sustainable Energy Reviews, 2009, pp. 428–438.

[8] B. Tammelin, M. Stuke, H. Seifert and S. Kimura, Icing effect on power production of wind turbines, Proceedings of the BOREAS IV Conference, Finland, 1998.

[9] C. Hochart, G. Fortin, J. Perron and A. Ilinca, Wind turbine performance under icing conditions, vol. 11, Wind Energy, 2008, pp. 319–333.

[10] M. Dimitrova, H. Ibrahim, G. Fortin, A. Ilinca and J. Perron, Software tool to predict the wind energy production losses due to icing, Electrical Power and Energy Conference (EPEC), 2011 IEEE, Winnipeg, MB, 2011, pp. 462–467.

[11] C. Mayer, A. Ilinca, G. Fortin and J. Perron, Design characteristics of electro-thermal deicing systems for wind turbine blades based on wind tunnel studies, vol. 17, International Journal of Offshore and Polar Engineering, 2007, pp. 182–188.

[12] O. Parent and A. Ilinca, Anti-icing and de-icing techniques for wind turbines: Critical review. Cold regions science and technology, 2011, vol. 65, no 1, p. 88–96.

[13] A. Ilinca, Analysis and Mitigation of Icing Effects on Wind Turbines, Wind Turbines, Dr. Ibrahim AlBahadly (Ed.), ISBN: 978-953-307-221-0, InTech. 2011.

[14] L. Makkonen, Estimating intensity of atmospheric ice accretion on stationary structures, vol. 20, Journal of Applied Meteorology, 1981, pp. 595–600.

[15] G. Fortin, J. Laforte and A. Ilinca, Heat and mass transfer during Ice accretion on aircraft wings with an improved roughness model, vol. 45, International Journal of Thermal Sciences, 2006, pp. 595–606.

[16] F. Villalpando, M. Reggio and A. Ilinca, Numerical study of flow around an iced wind turbine airfoil, vol. 6(1), Engineering Application of Computational Fluid Mechanics, pp. 39–45, 2012.

[17] L. Battisti, Wind turbines in cold climates: icing impacts and mitigation systems, ISBN: 978-3-319-05191-8, Switzerland: Springer International Publishing, 2015.

[18] O. Meier and D. Scholz, A Handbook Method for the Estimation of Power Requirements for Electrical De-Icing Systems. Deutscher Luft-und Raumfahrtkongress,

Hamburg, 2010. DocumentID: 161191. [Online]. Available: http://MOZART.Prof-Scholz.de [Accessed: 09 May 2016]

[19] J. Jonkman, S. Butterfield, W. Musial, and G. Scott, Definition of a 5-MW Reference Wind Turbine for Offshore System Development, NREL/TP-500-38060, Golden, CO: National Renewable Energy Laboratory, February 2009. DOI: 10.2172/947422

[20] P. Gipe, Wind energy basics: a guide to home and community-scale wind-energy systems, ISBN: 978-160-358-227-8, VT: Chelsea Green Publishing, 2009.

[21] Vestas, V120-4.5 MW Offshore leadership, Denmark: Vestas Wind Systems A/S, 2008. [Online]. Available: NRG Systems, http://www.nrg-systems.hu/dok/en/V120_UK.pdf [Accessed: 09 May 2016]

[22] Vestas, V100-2.75 MW The future for low wind sites, Denmark: Vestas Wind Systems A/S, 2008. [Online]. Available: NRG Systems, http://www.nrg-systems.hu/dok/en/V100_UK.pdf [Accessed: 09 May 2016]

[23] Vestas, V90 3.0 MW, Denmark: Vestas Wind Systems A/S, 2016. [Online]. Available: Direct Industry, https://www.vestas.com/en/products/turbines/v90-3_0_mw [Accessed: 09 May 2016]

[24] Vestas, V80-2.0 MW Versatile megawattage, Denmark: Vestas Wind Systems A/S, 2012. [Online]. Available: Vestas, http://pdf.directindustry.com/pdf/vestas/v80-20-mw-brochure/20680-53605.html [Accessed: 09 May 2016]